EFEMP1, S1-5, or FBNL) causes an inherited macular degenerative disease termed malattia leventinese or Doyne honeycomb retinal dystrophy (51). Missense variations in other fibulins have been detected in patients with age-related macular degeneration (47, 50), the most common cause of incurable blindness (6). Mutations in fibulin-5 have also been found in some cutis laxa patients (29, 32). So far, fibulin-5 is the only fibulin reported to be necessary for elastogenesis, whereas fibulin-1-null mice are reported to die perinatally as a result of hemorrhages, due to defects associated with capillary endothelial cells (25). Knockout mice for other fibulins have not been reported. Among the fibulins, fibulin-3, fibulin-4 (also known as EFEMP2, MBP1, H411, or UPH1), and fibulin-5 share highest homology with each other. These three fibulins are the smallest members of the family, share >50% amino acid identity, and are nearly identical in their structural organization (1, 10, 15, 52). Despite this homology, fibulin-5 deficiency is not compensated for by fibulin-3 or -4, suggesting that fibulin-3, -4, and -5 are not functionally redundant.

The function of fibulin-4 is poorly understood. Several studies have consistently found that fibulin-4 promotes cell growth, exhibits oncogenic properties, and is upregulated in tumor tissues (14, 16, 19). *fibulin-4* mRNA has been shown to be widely expressed in various tissues throughout the body (14, 16, 18). High protein levels are present in blood vessel walls (18). During development, *fibulin-4* mRNA is expressed in mouse embryos as early as embryonic day 7 (E7) (14). In this study, we investigated the biological role of fibulin-4 through targeted gene inactivation in mice. Remarkably, mice lacking fibulin-4 do not form elastic fibers, with resulting severe vascular and lung defects; they die perinatally. These results demonstrate that fibulin-4 plays an irreplaceable role in elastic fiber formation.

MATERIALS AND METHODS

***fibulin-4*$^{-/-}$ mouse generation, Southern blot analysis, and RT-PCR.** The targeting vector was constructed using 2.5-kb (5′) and 3-kb (3′) mouse *fibulin-4* genomic DNA fragments as homology arms. The two arms flanked a promoterless *lacZ* and a neomycin-resistant gene cassette (*lacZ-neo*). Homologous recombination in mouse embryonic stem cells resulted in the insertion of the *lacZ-neo* cassette into exon 4 of the mouse *fibulin-4* locus. Germ line-transmitting chimeric mice generated from the targeted embryonic stem cells were bred with C57BL/6 mice to produce F_1 *fibulin-4*$^{+/-}$ mice (Deltagen). Intercrossing of heterozygous F_1 mice generated F_2 *fibulin-4*$^{-/-}$ mice. Southern blot analysis was performed for identification of homologous recombinants. Genomic DNA was extracted using a DNA purification kit (Gentra) from mouse tail biopsy samples, digested with KpnI, separated on a 0.5% SeaKem Gold agarose (Cambrex) gel, and transferred to a Hybond-N$^+$ nylon membrane (Amersham) by capillary blotting. The membrane was hybridized with a 5′ or 3′ external probe that is outside of the homologous arm regions. The probes were labeled with ^{32}P through random priming using the Megaprime DNA Labeling system (Amersham). The labeled probes were purified using ProbeQuant G-50 Micro Columns (Amersham). Hybridization was performed using the MiracleHyb hybridization solution (Stratagene) according to the manufacturer's instructions. Reverse transcription-PCR (RT-PCR) was performed as described previously (33) to confirm the absence of *fibulin-4* expression in homozygous mice. Total RNA was isolated from wild-type, *fibulin-4*$^{+/-}$, and *fibulin-4*$^{-/-}$ mice at postnatal day 1 (P1). Either a 5′ or 3′ primer set corresponding to mouse *fibulin-4* cDNA sequence was used in the PCRs. The 5′ primer set (5′-GGCCAGATCTATGCTCCCTTT TGCCTCCTG-3′ and 5′-ACATCCACACAGCTCTCCTG-3′) generates a 381-bp fragment, and the 3′ primer set (5′-TGTCGAGAGCAGCCTTCA TC-3′ and 5′-GGCCGTCGACTCAGAAGGTATAGGCTCCCAC-3′) generates a 357-bp fragment. *fibulin-3* primers were used in the positive control.

Morphological and histological analyses. Timed pregnant mice were sacrificed by CO_2 asphyxiation for collection of embryos at E9.5 to E18.5. P1 pups were sacrificed by cervical dislocation. Sacrificed embryos or P1 mice were immobilized on agarose plates on their back. The ventral side of the embryos was gently dissected away to expose the aorta and other large arteries. Blood vessels were photographed with a dissecting microscope equipped with a charge-coupled device camera.

For histology, whole embryos and tissues dissected from newborn pups were fixed in Bouin's fixative or 4% paraformaldehyde in 0.1 M phosphate buffer (pH 7.2), dehydrated, and embedded in paraffin. Ten-micrometer sections were stained with hematoxylin and eosin or for elastin using elastin van Gieson stain (Sigma).

Transmission electron microscopy. Dissected tissues were fixed overnight in 3% glutaraldehyde in 0.144 M cacodylate buffer, pH 7.2. One-micrometer sections of plastic-embedded samples were cut and stained with methylene blue to examine the integrity of the tissue. Thin sections were cut on a Reichert Ultracut microtome, counterstained with uranyl acetate, and examined and photographed with a Philips CM-12S electron microscope.

Tissue desmosine assay. Tissue samples from P1 mice were collected from the thoracic aorta and lung. The tissues were hydrolyzed in 6 N HCl at 100°C for 24 h, evaporated to dryness, and redissolved in water. Desmosine was quantified by radioimmunoassay as previously described (49), and hydroxyproline was determined by amino acid analysis.

Northern blot analysis. Eight micrograms of total RNA isolated from various tissues of wild-type, *fibulin-4*$^{+/-}$, and *fibulin-4*$^{-/-}$ mice at P1 was separated on a 1% formaldehyde-agarose gel and transferred to a Hybond-XL nylon membrane (Amersham). Prehybridization was performed by incubating the membrane for 4 h at 65°C in the hybridization buffer without the probe. The membrane was hybridized with a ^{32}P-labeled probe using the Megaprime DNA Labeling system (Amersham). The *fibulin-4* probe is a 357-bp mouse *fibulin-4* cDNA fragment amplified by RT-PCR, the tropoelastin probe is a 3.6-kb mouse tropoelastin cDNA fragment containing the entire coding sequence released by SalI/NotI digestion from vector pCMV-SPORT6-mELN (Open Biosystems), and the LOX probe is a 4-kb mouse *Lox* cDNA fragment released by SalI-NotI digestion from vector pCMV-SPORT6-mLOX (Open Biosystems). After the *fibulin-4* probe was used, the same membranes were stripped by being boiled for 30 min in 0.1% sodium dodecyl sulfate (SDS), washed, and hybridized with other probes. A mouse glyceraldehyde-3-phosphate dehydrogenase (GAPDH) probe was used as a control. A 1.2-kb GAPDH fragment was generated by RT-PCR using the primers 5′-CCGCATCTTCTTGTGCAGTGCCA-3′ and 5′-CGAACTTTATTG ATGGTATTCAAGAGA.

Production of MAbs against human fibulin-4. cDNA encoding human fibulin-4 (OriGene Technologies) without signal peptide was cloned into vector pGEX-4T-2 (Pharmacia) to generate fibulin-4 fused with glutathione *S*-transferase (GST). GST–fibulin-4 or GST was purified as described previously (36). Four mice were immunized with GST–fibulin-4. Sera (polyclonal antibodies) from all the mice were characterized with both GST fusion proteins and lysates of transfected 293T cells expressing recombinant fibulin-4. Hybridomas were derived from one of these mice. Several different clones producing monoclonal antibodies (MAbs) against fibulin-4 were identified by enzyme-linked immunosorbent assay. Clones 7B9 (immunoglobulin G2a [IgG2a]) and 11E2 (IgG2b) are of high specificity and titer.

Transfection, immunoprecipitation, and immunoblotting. 293T cells were transfected with a control plasmid, pCMV6-XL4-fb4 (human *fibulin-4* cDNA), pCMV6-XL6-heln (human *tropoelastin* cDNA obtained from Origene), or both pCMV6-XL4-fb4 and pCMV6-XL6-heln with Lipofectamine (Invitrogen). At 48 h after transfection, cells were lysed. Immunoprecipitation and immunoblotting using antibodies against fibulin-4 and human elastin (Elastin Products Company) were performed as previously described (34) with modifications. To avoid the interference of the IgG heavy chain in interpreting results of immunoblotting following immunoprecipitation by the same or similar antibodies, immunoprecipitation was performed with antibodies covalently coupled to protein A-Sepharose. Anti-fibulin-4 MAb 7B9 or a rabbit anti-human tropoelastin polyclonal antibody (Elastin Products Company) was cross-linked to protein A-Sepharose CL-4B (Pharmacia) using dimethylpimelimidate (Sigma) as previously described (35). For each immunoprecipitation, cell lysate containing 200 μg of total protein was diluted to 1 ml with lysis buffer containing 50 mM Tris (pH 8.0), 150 mM NaCl, 10% glycerol, 0.5% NP-40, 0.5% Triton X-100, 1 mM phenylmethylsulfonyl fluoride, and a 1:100 dilution of protease inhibitor mixture III (Calbiochem). A total of 25 μl of antibody-protein A beads was incubated with the cell lysate for 4 h at 4°C. The immunoprecipitates were washed and resuspended in 30 μl of SDS-polyacrylamide gel electrophoresis (SDS-PAGE) sample buffer; 10 μl of the suspension was loaded to each well, resolved by SDS-PAGE on a 10% gel, and transferred onto a polyvinylidene difluoride membrane (Millipore). Anti-fibulin-4 MAb 11E2 or the anti-human tropoelastin antibody was used in immu-

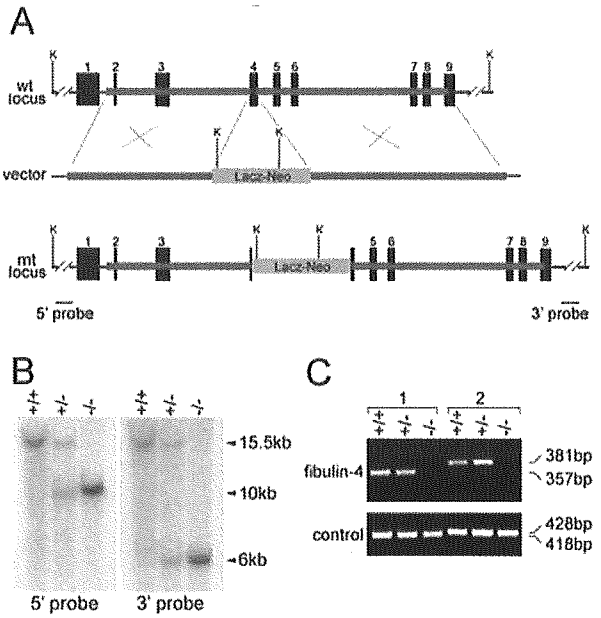

FIG. 1. Targeted disruption of the mouse *fibulin-4* gene. (A) Targeting strategy. Thick lines represent the homology arms used for constructing the targeting vector. Numbered solid boxes depict *fibulin-4* exons. The external 5′ and 3′ probes (B) are indicated as two bars beneath the mutant (mt) locus. wt, wild-type; K, KpnI. (B) Southern blot analysis of tail genomic DNA from wild-type (+/+), heterozygous (+/−), and homozygous (−/−) mice. The 15.5-kb wild-type band was detected by both 5′ and 3′ probes, the 10-kb mutant band was detected by the 5′ probe, and the 6-kb mutant band was detected by the 3′ probe. (C) RT-PCR analysis of mouse RNA. No PCR product was detected for homozygous mice with either a 3′ (1) or 5′ (2) primer set, indicating the absence of *fibulin-4* mRNA in these mice. In the positive control, PCR products were detected for all mice when a 3′ or 5′ primer set was used for fibulin-3.

noblotting. Alkaline phosphatase-conjugated anti-mouse IgG2b or anti-rabbit IgG (Jackson ImmunoResearch Laboratories) was used as a secondary antibody.

Production of recombinant fibulin-4 and solid-phase binding assay. Plasmid pEF6/V5 (Invitrogen) was modified to place a preprotrypsin signal sequence, a FLAG tag, and a His_6 tag to the N terminus of its inserted protein. Mouse *fibulin-4* cDNA without the signal sequence was subcloned to the modified vector. 293T cells were transfected with the resulting vector with Lipofectamine Plus (Invitrogen), according to the manufacturer's protocol. Stably transfected cells were selected with Blasticidin (Invitrogen). Recombinant fibulin-4 was purified from the serum-free conditioned medium of stable lines with TALON His-Tag Purification resins (Clontech) according to the manufacturer's instructions. The purity of the protein was confirmed by Coomassie blue staining of a SDS-PAGE gel, and the protein concentration was determined with Coomassie Plus reagent (Pierce). Various concentrations of purified fibulin-4 in Tris-buffered saline containing 2% skim milk with 2 mM $CaCl_2$ or 5 mM EDTA were used as ligands for a solid-phase binding assay. Recombinant bovine tropoelastin was prepared as previously described (26). Solid-phase binding assays using purified tropoelastin were performed as previously described (54) with the modification of 2 mM $CaCl_2$ or 10 mM EDTA added in the buffer. Anti-FLAG M2 antibody (Sigma) (1:2,000) was used as a primary antibody; horseradish peroxidase-conjugated anti-mouse IgG antibody (Santa Cruz) (1:3,000) was used as a secondary antibody. A color reaction assay was performed with the R&D Substrate Reagent Pack, followed by optic density measurement at 450 nm.

Cell culture and immunostaining. Normal human skin fibroblasts were cultured in Dulbecco's modified Eagle's medium with 10% fetal bovine serum at a density of 8×10^4 cells per 1 well of 24-well plate (day 0). On day 3, the medium was changed to Dulbecco's modified Eagle's medium-F12 with 10% fetal bovine serum and recombinant mouse fibulin-4 at a concentration of 5 μg/ml. On day 12, cells were fixed with 100% methanol and stained with rabbit antielastin antibody PR533 (1/100; Elastin Products Company) and mouse anti-FLAG M2 antibody (1/100; Sigma). Alexa Fluor 546-conjugated anti-rabbit IgG (1/100; Invitrogen) and Alexa Fluor 488-conjugated anti-mouse IgG (1/100; Invitrogen) were used as secondary antibodies. Stained cells were mounted with Vectashield with 4,6-diamino-2-phenylindole (DAPI) (Vector) and examined with a confocal microscope (Carl Zeiss).

RESULTS

Targeted inactivation of the *fibulin-4* gene results in perinatal lethality. The mouse *fibulin-4* gene was inactivated by insertion of a promoterless *lacZ* and a neomycin-resistant gene cassette into exon 4 (Fig. 1A). Homologous recombinants were identified by Southern blot analysis (Fig. 1B). The absence of *fibulin-4* mRNA was confirmed by RT-PCR (Fig. 1C) and Northern blot analysis (see Fig. 7). We found no adult homozygous offspring of *fibulin-4*$^{+/-}$ crossings, raising the possibility that ablation of fibulin-4 causes early lethality. Genotype analysis of offspring at several developmental stages indicated that the number of wild-type, heterozygous, and homozygous animals were distributed in a normal Mendelian pattern at embryonic stages E11.5 and E18.5 (Table 1). However, most *fibulin-4*$^{-/-}$ mice died during birth, only 10% survived to P1, and all the homozygous mice died by P2 (Table 1). The frequency of heterozygous animals was about twice that of the wild type and thus was not affected by the disruption of one *fibulin-4* allele. These results demonstrate that lack of fibulin-4 causes perinatal lethality in mice.

Severe vascular and lung defects in *fibulin-4*$^{-/-}$ mice. The gross appearances of wild-type, *fibulin-4*$^{+/-}$, and *fibulin-4*$^{-/-}$ mice at P1 were similar. However, on dissection, *fibulin-4*$^{-/-}$ mice exhibited severe vascular and lung defects. The arteries were tortuous, with irregularities including narrowing, dilatation, aneurysms, rupture, and resulting hemorrhages. The abnormalities were most severe in the aorta (Fig. 2B) and large arteries but occurred in other arteries as well. In addition, all live-born *fibulin-4*$^{-/-}$ mice were found to have expanded lungs. Histological examinations showed markedly enlarged distal airspaces, similar to those of emphysematous lungs (Fig. 2D). No obvious difference was observed in other organs. Despite the severe phenotype exhibited by homozygous animals, heterozygous (*fibulin-4*$^{+/-}$) mice are fertile, have a normal life span, and appear to be indistinguishable from the wild-type littermates.

The earliest abnormality appears in *fibulin-4*$^{-/-}$ embryos at E12.5. To determine the onset time of defects in *fibulin-4*$^{-/-}$ mice, we studied different developmental stages of the mice. The earliest abnormality noted was a uniformly narrowing of the descending aorta in *fibulin-4*$^{-/-}$ embryos at E12.5 (Fig. 3B). The outer diameter of the aorta in *fibulin-4*$^{-/-}$ mice was only

TABLE 1. Genotype frequency of offspring from *fibulin-4*$^{+/-}$ mouse breedings

Stage	No. of animals (%) of genotype:			Total no.
	+/+	+/−	−/−	
E11.5	16 (31)	23 (45)	12 (24)	51
E18.5	18 (21)	45 (52)	23 (27)	86
P1	33 (32)	61 (59)	10 (10)	104
P2	46 (32)	97 (67)	1 (<1)	144
P3	53 (31)	118 (69)	0	171

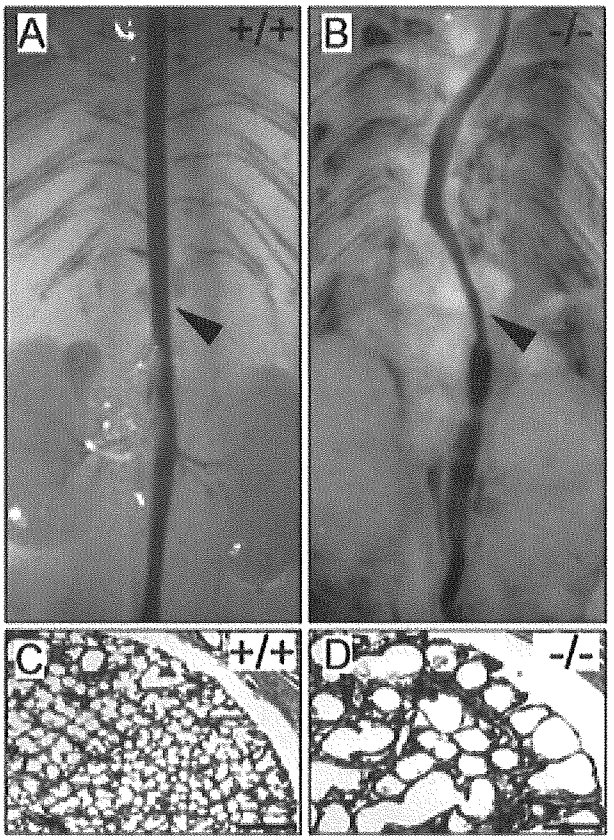

FIG. 2. Aorta and lung defects in *fibulin-4*$^{-/-}$ mice. (A and B) Aorta (arrowheads) of *fibulin-4*$^{+/+}$ and *fibulin-4*$^{-/-}$ mice at P1. (C and D) Hematoxylin and eosin staining of lung sections from mice at P1. The airspaces are significantly enlarged in *fibulin-4*$^{-/-}$ mice. Scale bars, 400 μm.

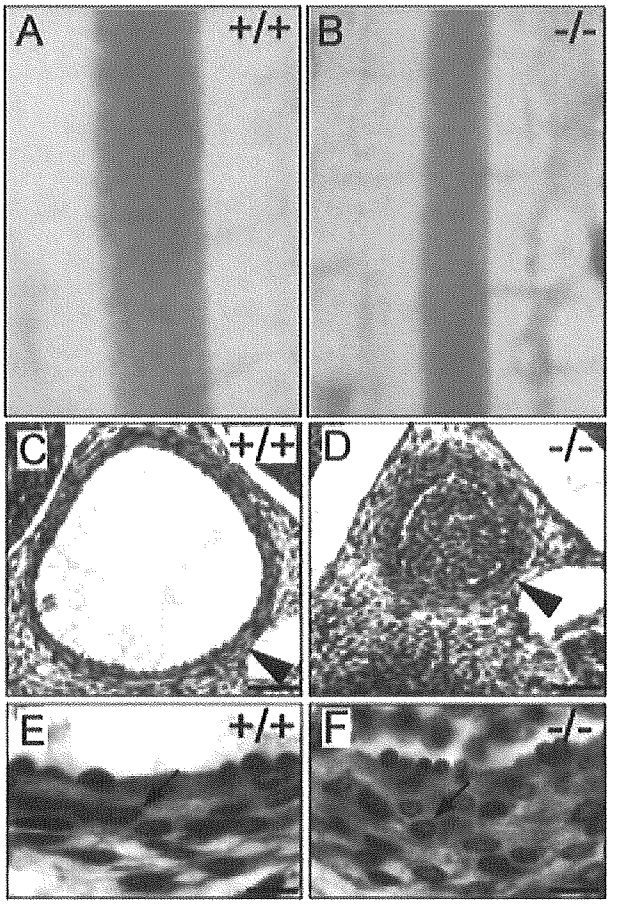

FIG. 3. The earliest abnormality in *fibulin-4*$^{-/-}$ mice at E12.5. (A and B) Aortas of *fibulin-4*$^{+/+}$ and *fibulin-4*$^{-/-}$ embryos at E12.5. (C to F) Hematoxylin and eosin staining of cross sections of descending aorta from E12.5 embryos. Note the smaller diameter and thicker wall of the *fibulin-4*$^{-/-}$ aorta (D). In contrast to the elongated, spindle-shaped cells (E, arrow) in wild-type mice, aortic wall cells were round in the *fibulin-4*$^{-/-}$ mice (F, arrow). Scale bars, 50 μm (C and D) and 20 μm (E and F).

one-half to two-thirds that of wild-type littermates. Histological analyses of cross sections showed that the aortic walls of *fibulin-4*$^{-/-}$ mice were nearly twice as thick as those of wild-type mice (Fig. 3D). However, the thickening of the *fibulin-4*$^{-/-}$ aortic wall did not appear to be the result of subendothelial overproliferation of cells, as the number of cells was similar in both *fibulin-4*$^{-/-}$ and wild-type aortic wall cross sections. There were 193 ± 3 cells for the wild type (data represent means and standard deviations for results with four mice) and 188 ± 7 cells for the homozygote (four mice) in a cross section of the aortic wall at a similar level of the thoracic aorta as shown in Fig. 3C and D. In contrast to the elongated and spindle-shaped cells in wild-type mice (Fig. 3E), the *fibulin-4*$^{-/-}$ aortic smooth muscle cells were round and appeared to be less stretched (Fig. 3F). The narrowing and the cell shape difference of the *fibulin-4*$^{-/-}$ aorta became less obvious at E13.5 and at older embryonic ages, likely due to passive expansion of the aorta caused by the dramatic increase in systemic blood pressure during these stages (22). Aortic tortuosity and irregularity were noticeable at E15.5 and became more pronounced with age in homozygous animals. These aorta abnormalities were not observed in *fibulin-4*$^{+/-}$ embryos.

***fibulin-4*$^{-/-}$ mice do not form elastic fibers.** The vascular and lung abnormalities of *fibulin-4*$^{-/-}$ mice were suggestive of elastic fiber defects. The appearance of abnormalities, coincident with the onset of elastogenesis in mice, suggests that genesis of elastic fibers may be impaired in *fibulin-4*$^{-/-}$ mice. Thus, we stained tissue sections from E12.5 to P1 with elastin van Gieson staining, which specifically stains elastic fibers. In the wild type, the innermost elastic lamina of the aorta was identifiable at E13.5 under a light microscope (Fig. 4A). By E14.5, four elastic laminae could be distinguished (Fig. 4C). All five elastic laminae were present at E16.5 or older ages (Fig. 4E and G). In contrast, no continuous elastic lamina was observed in the *fibulin-4*$^{-/-}$ aorta at any stage (Fig. 4B, D, F, and H). Instead, irregular elastin aggregates were visible at E14.5 (Fig. 4D), and more and larger aggregates accumulated with age (Fig. 4F and H). In the lung and skin, elastic fibers were not distinguishable by light microscopy at any embryonic stages. At P1, fine elastic fibers could be observed in lung and the hypodermal connective tissue of the skin of wild-type mice (Fig. 5A and C) but not in *fibulin-4*$^{-/-}$ mice (Fig. 5B and D). Despite this, the skin of *fibulin-4*$^{-/-}$ mice did not show obvious

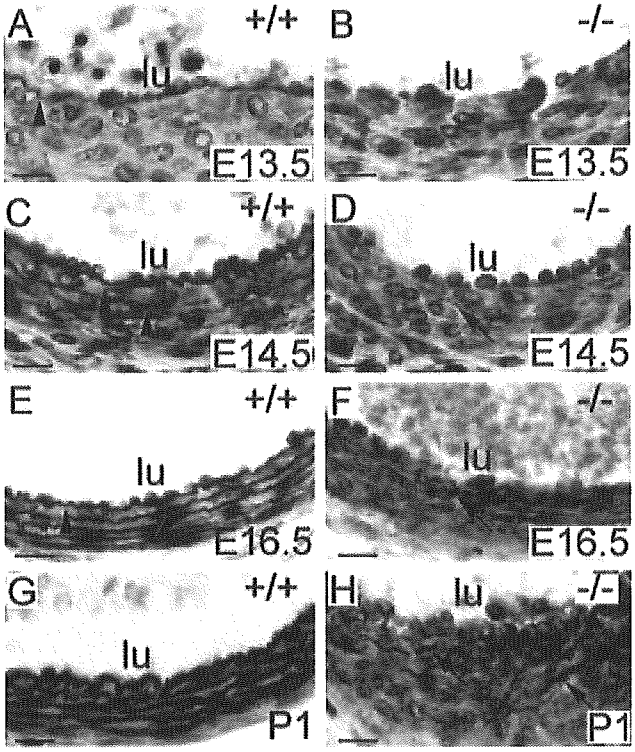

FIG. 4. Lack of elastic lamina in the *fibulin-4*$^{-/-}$ aorta. Elastin van Gieson staining of cross sections of descending aortae at different developmental stages is shown. The innermost elastic lamina (arrowheads) was identifiable in the wild-type aorta at E13.5 (A) and became more numerous and thicker at subsequent developing stages (C, E, and G). Only irregular elastin aggregates (arrows) were observed in the *fibulin-4*$^{-/-}$ aorta (B, D, F, and H). lu, lumen. Scale bars, 20 μm.

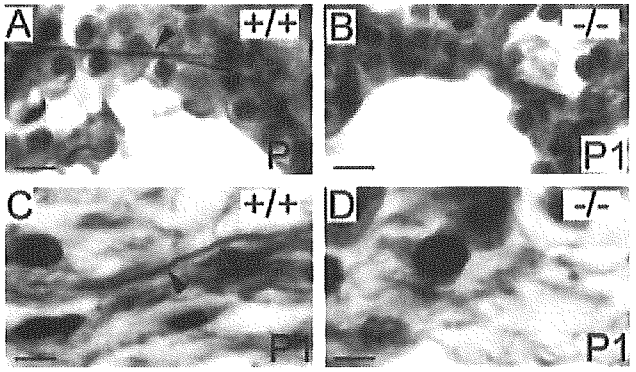

FIG. 5. Lack of elastic fibers in the skin and lung of *fibulin-4*$^{-/-}$ mice. (A and B) Elastin van Gieson staining of lung sections from P1 mice. Fine branched elastic fibers (arrowhead) were present in the wild-type (A) but not *fibulin-4*$^{-/-}$ (B) lung. (C and D) Elastin staining of skin sections from P1 mice. Elastic fibers were observed in the hypodermal connective tissue area of the wild-type skin (C, arrowhead) but not in the *fibulin-4*$^{-/-}$ skin (D). Scale bars, 10 μm (A and B) and 5 μm (C and D).

gross differences at this young age. Elastic fibers of *fibulin-4*$^{+/-}$ mice were similar to those of wild-type littermates. These results indicate that fibulin-4 is required for general elastogenesis.

Elastin aggregates containing electron dense rod-like filaments in *fibulin-4*$^{-/-}$ mice. To further understand the elastic fiber defects in *fibulin-4*$^{-/-}$ mice, we examined the aortae of E14.5 and P1 mice by electron microscopy (Fig. 6). Consistent with the finding by light microscopy, no intact elastic lamina was observed in the *fibulin-4*$^{-/-}$ aorta at either E14.5 or P1. Continuous elastic lamina was present in the wild-type aorta (Fig. 6A and C), but only irregular elastin aggregates were found in the *fibulin-4*$^{-/-}$ aorta at both stages (Fig. 6B and D, arrows). Noticeably, the content of the elastin aggregates appeared to be different from that of normal elastic fibers. Instead of an amorphous content, these elastin aggregates contained distinguishable electron-dense substances. Under higher magnification, dark rod-like filaments with similar sizes were seen to be evenly distributed in the elastin aggregates (Fig. 6F). These findings demonstrate that elastin does not properly assemble without fibulin-4.

Desmosine content is severely reduced in *fibulin-4*$^{-/-}$ mice. To determine whether mature elastin content is affected in *fibulin-4*$^{-/-}$ mice, we assessed the level of desmosine, an elastin cross-link-specific amino acid, in the aorta and lungs of wild-type, heterozygous, and homozygous mutant mice. As shown in Table 2, elastin cross-linking was nearly absent in *fibulin-4*$^{-/-}$ mice. There was a 94% decrease in the amount of desmosine in the aorta and 88% decrease in lungs of *fibulin-4*$^{-/-}$ mice compared with wild-type mice. Interestingly, there was a near 20% increase in the amount of desmosine in heterozygous mutants compared with wild-type mice (Table 2), although this difference was not statistically significant ($P > 0.05$ in a t test). We did not find any difference in the level of hydroxyproline, an indicator of collagen content, between wild-type and *fibulin-4*$^{-/-}$ mice (data not shown), indicating that the amount of collagen did not differ in *fibulin-4*$^{-/-}$ mice.

Tropoelastin and LOX expression is not affected in *fibulin-4*$^{-/-}$ mice. Elastin cross-linking is catalyzed by LOX family enzymes. Among the five known members, LOX has been shown to be necessary for elastic fiber development (20, 31). To determine whether lack of fibulin-4 causes elastinopathy by affecting tropoelastin or *Lox* expression, we examined the mRNA levels of *fibulin-4*, tropoelastin, and *Lox* in wild-type, heterozygous, and homozygous littermates at P1. As shown in Fig. 7, while heterozygotes showed reduced *fibulin-4* mRNA levels compared to those in wild-type mice and homozygotes had no detectable *fibulin-4* mRNA, all of them had similar levels of tropoelastin or *Lox* expression. Elastin has been shown to have an antiproliferative effect on vascular smooth muscle cells, and mice lacking elastin (*ELN*$^{-/-}$) die of vascular occlusion resulting from subendothelial cell proliferation (27). The unaffected tropoelastin expression is consistent with the lack of cell overproliferation and the accumulation of irregular elastin aggregates in *fibulin-4*$^{-/-}$ mice.

Fibulin-4 interacts with tropoelastin and assembles into elastic fibers. To investigate possible mechanisms by which fibulin-4 affects elastogenesis, we assessed the potential for interaction between fibulin-4 and elastin. Recombinant mouse fibulin-4 was expressed and purified from stably transfected 293T cell medium (Fig. 8A). A FLAG tag and a His_6 tag were added at the N terminus of fibulin-4 without its signal peptide to facilitate the purification and characterization of fibulin-4.

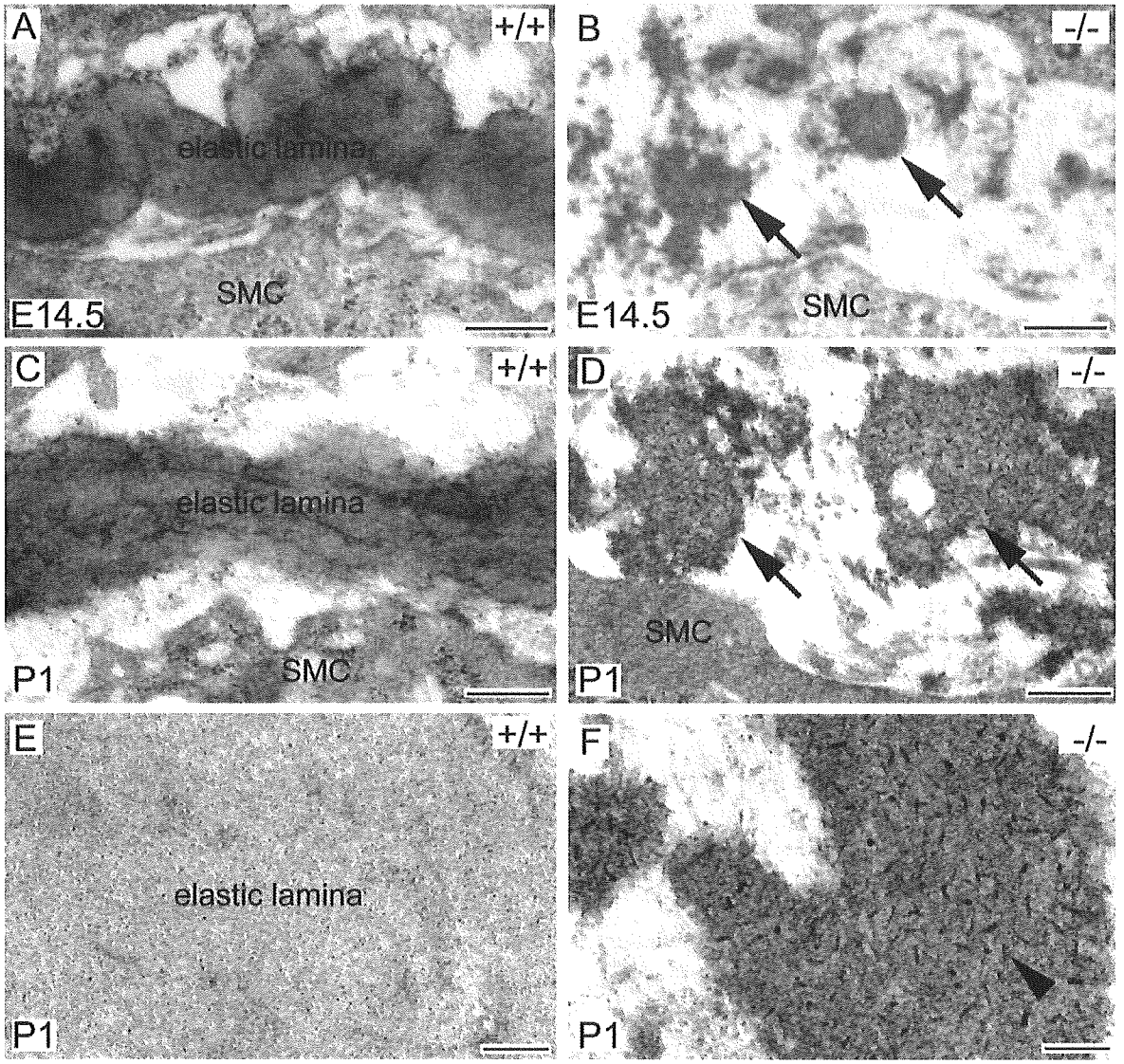

FIG. 6. Electron microscopy of elastic laminae in *fibulin-4*$^{-/-}$ mice. (A to D) Descending aorta cross sections from E14.5 (A and B) and P1 (C and D) mice. The wild-type aorta contained continuous elastic lamina (A and C). In contrast, irregular elastin aggregates (arrows) were randomly distributed in the *fibulin-4*$^{-/-}$ aorta (B and D). Under higher magnification (E and F), the wild-type elastic lamina appeared to be amorphous (E). But distinct, dark rod-like filaments (F, arrowhead) were evenly distributed in the *fibulin-4*$^{-/-}$ elastin aggregates. SMC, smooth muscle cell. Scale bars, 400 nm (A to D) and 100 nm (E and F).

The tagged protein was secreted from a preprotrypsin signal sequence. Although we found that untagged fibulin-4 was secreted efficiently from its native signal peptide, the C-terminal-tagged fibulin-4 was poorly secreted. It is possible that the C-terminal domain affects protein folding and is sensitive to modification. In a solid-phase binding assay, purified tropoelastin was used as an immobilized protein substrate, and fibulin-4 was used as a soluble ligand. As shown in Fig. 8B, fibulin-4 bound strongly to tropoelastin in the presence of Ca^{2+} and the binding was inhibited in the presence of EDTA, suggesting that calcium is required for the binding and the calcium-binding epidermal growth factor domains of fibulin-4 may be necessary for this binding. However, it has not been demonstrated experimentally that fibulin-4 binds calcium. No binding was observed between fibulin-4 and a control substrate (bovine serum albumin). These results indicate that fibulin-4 and tropoelastin can interact directly.

TABLE 2. Desmosine in picomoles per milligram of protein in aorta and lung at P1

Genotype (n)	Desmosine ± SD (% of wild type) in:	
	Aorta	Lung
+/+ (12)	419.05 ± 125.94 (100)	29.7 ± 14.87 (100)
+/− (21)	501.86 ± 133.85 (120)[a]	35.63 ± 9.08 (120)[b]
−/− (6)	25.35 ± 8.69 (6)[c]	3.15 ± 1.45 (12)[c]

[a] $P = 0.09$, compared to the wild type by t test.
[b] $P = 0.23$, compared to the wild type by t test.
[c] $P < 0.0001$, compared to the wild type by t test.

To assess whether fibulin-4 and tropoelastin interact in solution, we performed a coimmunoprecipitation assay. Human *fibulin-4* cDNA, human *tropoelastin* cDNA, or both were trans-

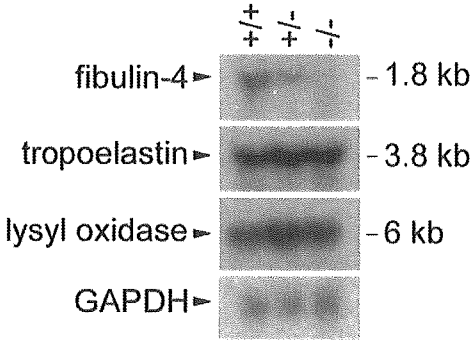

FIG. 7. Unaffected tropoelastin and lysyl oxidase expression in *fibulin-4*$^{-/-}$ mice. Northern blot analysis of equal amount of mouse lung total RNA shows a *fibulin-4* mRNA transcript of 1.8 kb detectable in wild-type (+/+) and heterozygous (+/−) but not homozygous (−/−) mice (top). The intensity of the signal is reduced in heterozygous mice. The same blot stripped and reblotted with a tropoelastin probe shows a 3.8-kb tropoelastin transcript with similar intensity in all the mice (second panel from the top). Probing with a *Lox* probe indicates a 6-kb *Lox* transcript with similar levels in all mice (third panel). A GAPDH probe was used as a control (bottom).

fected into 293T cells. Tropoelastin was expressed at a very low level. We could detect tropoelastin in the cell lysate, but it was difficult to detect it in the culture medium, presumably due to its self-coacervation and formation of insoluble elastin in the medium. Fibulin-4 was expressed at a relatively high level and could be readily detected in both lysate and medium. Thus, we chose to use transfected cell lysates for the coimmunoprecipitation assay. As shown in Fig. 8C, tropoelastin was immunoprecipitated from lysates transfected with either tropoelastin alone (lane 2) or both tropoelastin and fibulin-4 (lane 1) by the antitropoelastin antibody. It was also coimmunoprecipitated by an anti-fibulin-4 monoclonal antibody from the lysate cotransfected with tropoelastin and fibulin-4 (lane 3). The coimmunoprecipitation did not appear to be due to a nonspecific association of tropoelastin with the fibulin-4 antibody beads, as no tropoelastin signal was detected from the immunoprecipitate by the same antibody from the lysate transfected only with tropoelastin (lane 4). Reciprocally, fibulin-4 was coimmunoprecipitated by the anti-tropoelastin antibody from the lysate transfected with both tropoelastin and fibulin-4 (lane 7) but not from the lysate transfected with fibulin-4 alone (lane 8), while it was immunoprecipitated by the fibulin-4 antibody from both lysates (lanes 5 and 6). These results demonstrate that fibulin-4 binds specifically with tropoelastin.

To further determine whether exogenous fibulin-4 is colocalized to elastic fibers, we added FLAG-tagged recombinant fibulin-4 to cultured human fibroblasts. These cells are capable of developing a network of elastic fibers in vitro. Double labeling of antitropoelastin and anti-FLAG antibodies showed colocalization of fibulin-4 and elastin (Fig. 9). These data indicate that fibulin-4 assembles into elastic fibers.

DISCUSSION

Elastic fiber formation is thought to involve extrinsic proteins and an intrinsic capacity for elastin coacervation. How extrinsic proteins cooperate with each other and with elastin coacervation to form functional elastic fibers is unknown. Over 30 molecules have been reported to associate with elastic fibers in morphological studies and in vitro assays (23). But many

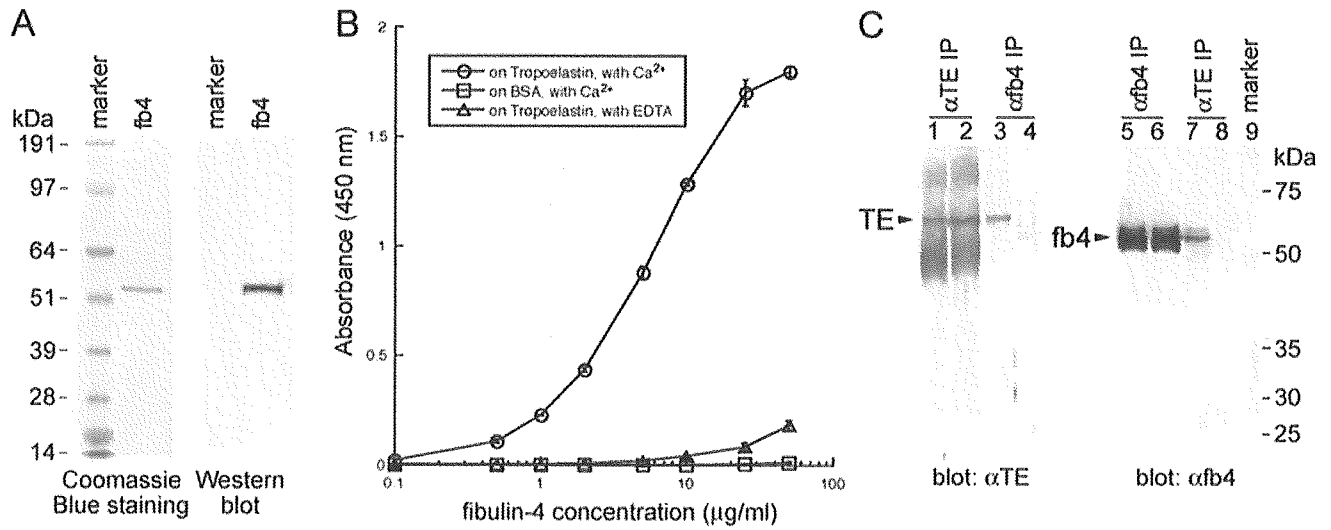

FIG. 8. Fibulin-4 interacts with tropoelastin. (A) Purified recombinant mouse fibulin-4. A total of 1 μg of purified fibulin-4 was used for the Coomassie blue-stained gel, and 10 ng of the protein was used for the Western blot. An anti-FLAG antibody was used for immunodetection. A single band with the correct mass for fibulin-4 was detected by both Coomassie blue staining and immunoblotting. (B) Solid-phase binding assay using recombinant fibulin-4 as a soluble ligand. Note that fibulin-4 binds to tropoelastin in the presence of Ca^{2+} but that the binding is inhibited in the presence of EDTA. Data were obtained as the results of triplicate experiments, and values shown are means ± standard deviations. (C) Coimmunoprecipitation of fibulin-4 with tropoelastin. Lanes 1 to 4, antitropoelastin blotting of immunoprecipitates from lysates of 293T cells transfected with both tropoelastin and fibulin-4 (lanes 1 and 3) or tropoelastin alone (lanes 2 and 4). Tropoelastin was detected in the immunoprecipitate by anti-fibulin-4 (7B9) (lane 3). Lanes 5 to 8, anti-fibulin-4 (11E2) blotting of immunoprecipitates from lysates of 293T cells transfected with both tropoelastin and fibulin-4 (lanes 5 and 7) or fibulin-4 alone (lanes 6 and 8). Fibulin-4 was detected in the immunoprecipitate by antitropoelastin (lane 7). IP, immunoprecipitation; TE, tropoelastin; fb4, fibulin-4.

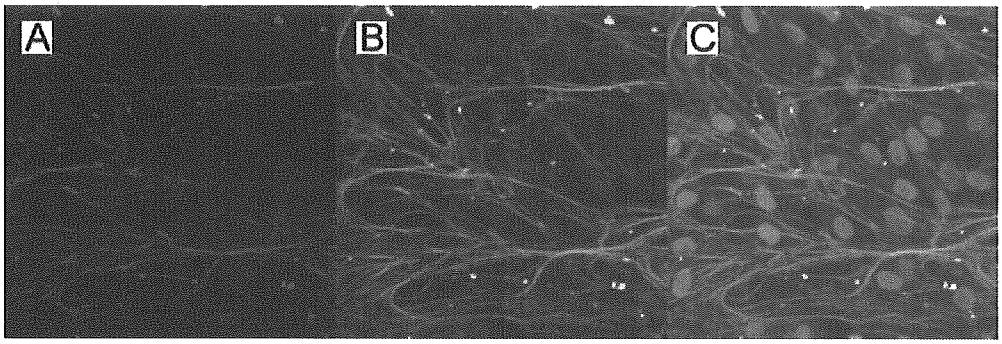

FIG. 9. Colocalization of fibulin-4 and elastin. (A to C) Normal human skin fibroblasts were cultured with FLAG-tagged recombinant fibulin-4 protein. (A) Cells stained with antitropoelastin antibody, showing a network structure. (B) Cells stained with anti-FLAG antibody, also showing a network structure. (C) Superimposed image of panels A and B, with DAPI nuclear staining showing fibulin-4 localization on elastic fibers.

have been found to have no effect or marginal effects on elastic fiber formation in vivo. In this study, we demonstrated that mice lacking fibulin-4 do not form elastic fibers. This is the first report that lack of a protein other than elastin itself completely abolishes the formation of elastic fibers in vivo, indicating that fibulin-4 plays an indispensable role in elastogenesis.

The initial abnormality present in *fibulin-4*$^{-/-}$ mice, arterial narrowing, is similar to that observed with *ELN*$^{-/-}$ mice (27). In *ELN*$^{-/-}$ mice, however, the change is caused by subendothelial cell overproliferation due to the lack of elastin, a process that eventually obliterates the vascular lumen (27). In *fibulin-4*$^{-/-}$ mice, tropoelastin mRNA levels are similar to those in wild-type mice, there is no sign of cell overproliferation and vascular occlusion, and irregular elastin aggregates accumulate with age, suggesting that fibulin-4 does not affect the synthesis of tropoelastin. The formation of functional elastic fibers requires the deposition of tropoelastin at the fiber assembly site, cross-linking of tropoelastin monomers by lysyl oxidase family enzymes, and the organization of resulting insoluble elastin matrix into mature fibers. Fibulin-4 likely affects one or more of these processes.

The irregular elastin aggregates observed in *fibulin-4*$^{-/-}$ mice are highly unusual in that they contain electron-dense rod-like filaments. These filaments are evenly distributed in the aggregates in *fibulin-4*$^{-/-}$ mice, as if, without fibulin-4, a molecule(s) associated with tropoelastin is incorporated together with each tropoelastin monomer into elastin aggregates. Alternatively, the rod-like filament may be a regular elastic fiber component whose presence is revealed by the absence of fibulin-4. The morphology of *fibulin-4*$^{-/-}$ elastin aggregates is similar to that of abnormal elastin aggregates permeated by proteoglycans in the presence of lysyl oxidase inhibitors (13). Also, ECM proteoglycans containing sulfated glycosaminoglycans visualized by a cationic copper phthalocyanin dye, cupromeronic blue, exhibit morphology very similar to the rod-like filaments observed in irregular elastin aggregates in *fibulin-4*$^{-/-}$ mice (48). These observations suggest that the filaments in *fibulin-4*$^{-/-}$ elastin aggregates may be proteoglycans. Glycosaminoglycans containing sulfate groups (chondroitin, dermatan, and heparan sulfate) and their associated proteoglycans have been shown to directly interact with tropoelastin and are normal components of elastic fibers (3, 7, 17, 55). Both chondroitin sulfate and heparan sulfate can mediate tropoelastin's coacervation (17, 24, 45, 53, 55). Decreased elastin deposition was observed when the matrix was depleted of sulfated molecules by chlorate treatment of the cells (8, 53). We also found that fibulin-4 interacts with tropoelastin directly and assembles into elastic fibers in culture. Thus, fibulin-4 may play a role in the initial deposition of tropoelastin, such as scaffolding and facilitating the formation of homogeneous elastin polymers by preventing the association of other molecules with tropoelastin or coordinating tropoelastin and other elastic fiber components during elastic fiber assembly. The identity of the rod-like filaments, the precise roles of proteoglycans in elastogenesis, and their relationships with fibulin-4 remain to be determined.

Elastin cross-linking is severely affected in *fibulin-4*$^{-/-}$ mice. Desmosine was reduced by over 85% in *fibulin-4*$^{-/-}$ mice, compared to levels in wild-type mice. Interestingly, there was a near-20% increase in desmosine in *fibulin-4*$^{+/-}$ mice compared to wild-type mice, although this difference was not statistically significant with the number of animals we analyzed. It is possible that there is more cross-linking in heterozygous mutants than in wild-type mice to compensate for fibulin-4 haploinsufficiency. Elastin cross-linking is catalyzed by lysyl oxidases, a family of enzymes that catalyzes the oxidative deamination of lysine residues in elastin and collagen (21). Five members have been described so far (12, 30). LOX has been shown to be necessary for elastic fiber and collagen fiber development (20, 31), and LOX-like 1 (LOXL1) is required in elastic fiber homeostasis (28). Similar to *fibulin-4*$^{-/-}$ mice, *Lox*$^{-/-}$ mice exhibit severe vascular defects and die perinatally (20, 31). The vascular defects include artery tortuosity, irregularity, and ruptured aneurysms with fragmented elastic lamina in the aortic walls. Desmosine content is decreased by 60%; hydroxyproline, which represents collagen content, is decreased by 30% in *Lox*$^{-/-}$ mice (20). The similarities in gross defects between *fibulin-4*$^{-/-}$ mice and *Lox*$^{-/-}$ mice and loss of desmosine content in *fibulin-4*$^{-/-}$ mice suggest that lack of fibulin-4 may affect the function of lysyl oxidase. However, *Lox* mRNA expression is similar in wild-type and *fibulin-4*$^{-/-}$ mice, hydroxyproline content is not altered in *fibulin-4*$^{-/-}$ mice, and no unusual elastic fiber content such as rod-like filaments found in *fibulin-4*$^{-/-}$ mice has been reported with *Lox*$^{-/-}$ mice. Loxl1-null mice survive to adulthood but do not deposit normal elastic fibers in the uterine tract postpartum; they develop

pelvic prolapse, enlarged airspaces of the lung, loose skin, and vascular abnormalities. Desmosine content in *Loxl1*$^{-/-}$ mice is reduced by 30 to 50%, depending on tissues (28). The difference in elastic fiber defects in *fibulin-4*$^{-/-}$, *Lox*$^{-/-}$, and *Loxl1*$^{-/-}$ mice suggests that fibulin-4 has different roles in elastic fiber assembly, even if it also affects the activities of lysyl oxidases.

Fibulin-4 shares high homology with fibulin-5, with a similar domain structure and >50% amino acid identity. Fibulin-5-null mice grow to adulthood but exhibit loose skin, lung airspace enlargement, and a stiff and tortuous aorta, due to disorganized and fragmented elastic fibers (40, 56). It has been proposed that fibulin-5 may be involved in elastogenesis by tethering elastic fibers onto cell surface integrins and by affecting cross-linking of elastin through direct binding with LOXL1 (28, 40, 56). *Loxl1*$^{-/-}$ mice exhibit similar but less-severe elastic fiber defects than *fibulin-5*$^{-/-}$ mice. Despite the high homology between fibulin-4 and -5, the *fibulin-4*$^{-/-}$ phenotype is not compensated for by fibulin-5. *fibulin-4*$^{-/-}$ mice exhibited almost complete loss of elastic fibers and perinatal lethality, suggesting a more essential role of fibulin-4 in elastogenesis than that of fibulin-5.

With age and some pathological conditions, elastic fibers exhibit interwoven filaments (41) that are similar to the morphology of elastin aggregates of *fibulin-4*$^{-/-}$ mice. Thus, alteration of the function or structure of fibulin-4 may be a major mechanism behind aging and elastic fiber-related diseases. *fibulin-4*$^{-/-}$ mice exhibit the most severe elastinopathy described to date. Understanding the role of fibulin-4 is a prerequisite for understanding the mechanism responsible for elastogenesis. In addition to the crucial role in elastogenesis, fibulin-4 may also have other important functions in cell proliferation and differentiation. Several studies have found that fibulin-4 stimulates cell growth and is upregulated in tumors (14, 16, 19). *fibulin-4*$^{-/-}$ mice will also be a valuable model in further studying these functions.

ACKNOWLEDGMENTS

We thank Peggy McCuskey for electron microscopy and Anna Yocom for technical assistance.

This work was supported by NIH/NEI grants EY13847 and EY13160, Research to Prevent Blindness, Philip Morris USA and Philip Morris International, Health and Labor Sciences research grants, Japan Society for the Promotion of Science, and Japan Science and Technology Agency.

REFERENCES

1. **Argraves, W. S., L. M. Greene, M. A. Cooley, and W. M. Gallagher.** 2003. Fibulins: physiological and disease perspectives. EMBO Rep. **4:**1127–1131.
2. **Arteaga-Solis, E., B. Gayraud, S. Y. Lee, L. Shum, L. Sakai, and F. Ramirez.** 2001. Regulation of limb patterning by extracellular microfibrils. J. Cell Biol. **154:**275–281.
3. **Baccarani-Contri, M., D. Vincenzi, F. Cicchetti, G. Mori, and I. Pasquali-Ronchetti.** 1990. Immunocytochemical localization of proteoglycans within normal elastin fibers. Eur. J. Cell Biol. **53:**305–312.
4. **Bressan, G. M., I. Castellani, M. G. Giro, D. Volpin, C. Fornieri, and I. Pasquali Ronchetti.** 1983. Banded fibers in tropoelastin coacervates at physiological temperatures. J. Ultrastruct. Res. **82:**335–340.
5. **Bressan, G. M., I. Pasquali-Ronchetti, C. Fornieri, F. Mattioli, I. Castellani, and D. Volpin.** 1986. Relevance of aggregation properties of tropoelastin to the assembly and structure of elastic fibers. J. Ultrastruct. Mol. Struct. Res. **94:**209–216.
6. **Bressler, N. M., S. B. Bressler, and S. L. Fine.** 1988. Age-related macular degeneration. Surv. Ophthalmol. **32:**375–413.
7. **Broekelmann, T. J., B. A. Kozel, H. Ishibashi, C. C. Werneck, F. W. Keeley, L. Zhang, and R. P. Mecham.** 2005. Tropoelastin interacts with cell-surface glycosaminoglycans via its COOH-terminal domain. J. Biol. Chem. **280:**40939–40947.
8. **Buczek-Thomas, J. A., C. L. Chu, C. B. Rich, P. J. Stone, J. A. Foster, and M. A. Nugent.** 2002. Heparan sulfate depletion within pulmonary fibroblasts: implications for elastogenesis and repair. J. Cell Physiol. **192:**294–303.
9. **Chaudhry, S. S., J. Gazzard, C. Baldock, J. Dixon, M. J. Rock, G. C. Skinner, K. P. Steel, C. M. Kielty, and M. J. Dixon.** 2001. Mutation of the gene encoding fibrillin-2 results in syndactyly in mice. Hum. Mol. Genet. **10:**835–843.
10. **Chu, M. L., and T. Tsuda.** 2004. Fibulins in development and heritable disease. Birth Defects Res. C Embryo Today **72:**25–36.
11. **Cox, B. A., B. C. Starcher, and D. W. Urry.** 1974. Communication: coacervation of tropoelastin results in fiber formation. J. Biol. Chem. **249:**997–998.
12. **Csiszar, K.** 2001. Lysyl oxidases: a novel multifunctional amine oxidase family. Prog. Nucleic Acid Res. Mol. Biol. **70:**1–32.
13. **Fornieri, C., M. Baccarani-Contri, D. Quaglino, Jr., and I. Pasquali-Ronchetti.** 1987. Lysyl oxidase activity and elastin/glycosaminoglycan interactions in growing chick and rat aortas. J. Cell Biol. **105:**1463–1469.
14. **Gallagher, W. M., M. Argentini, V. Sierra, L. Bracco, L. Debussche, and E. Conseiller.** 1999. MBP1: a novel mutant p53-specific protein partner with oncogenic properties. Oncogene **18:**3608–3616.
15. **Gallagher, W. M., C. A. Currid, and L. C. Whelan.** 2005. Fibulins and cancer: friend or foe? Trends Mol. Med. **11:**336–340.
16. **Gallagher, W. M., L. M. Greene, M. P. Ryan, V. Sierra, A. Berger, P. Laurent-Puig, and E. Conseiller.** 2001. Human fibulin-4: analysis of its biosynthetic processing and mRNA expression in normal and tumour tissues. FEBS Lett. **489:**59–66.
17. **Gheduzzi, D., D. Guerra, B. Bochicchio, A. Pepe, A. M. Tamburro, D. Quaglino, S. Mithieux, A. S. Weiss, and I. Pasquali Ronchetti.** 2005. Heparan sulphate interacts with tropoelastin, with some tropoelastin peptides and is present in human dermis elastic fibers. Matrix Biol. **24:**15–25.
18. **Giltay, R., R. Timpl, and G. Kostka.** 1999. Sequence, recombinant expression and tissue localization of two novel extracellular matrix proteins, fibulin-3 and fibulin-4. Matrix Biol. **18:**469–480.
19. **Heine, H., R. L. Delude, B. G. Monks, T. Espevik, and D. T. Golenbock.** 1999. Bacterial lipopolysaccharide induces expression of the stress response genes hop and H411. J. Biol. Chem. **274:**21049–21055.
20. **Hornstra, I. K., S. Birge, B. Starcher, A. J. Bailey, R. P. Mecham, and S. D. Shapiro.** 2003. Lysyl oxidase is required for vascular and diaphragmatic development in mice. J. Biol. Chem. **278:**14387–14393.
21. **Kagan, H. M., and P. C. Trackman.** 1991. Properties and function of lysyl oxidase. Am. J. Respir. Cell Mol. Biol. **5:**206–210.
22. **Kaufman, M. H., and J. B. L. Bard.** 1999. The Anatomical basis of mouse development. Academic Press, London, United Kingdom.
23. **Kielty, C. M., M. J. Sherratt, and C. A. Shuttleworth.** 2002. Elastic fibres. J. Cell Sci. **115:**2817–2828.
24. **Kielty, C. M., S. P. Whittaker, and C. A. Shuttleworth.** 1996. Fibrillin: evidence that chondroitin sulphate proteoglycans are components of microfibrils and associate with newly synthesised monomers. FEBS Lett. **386:**169–173.
25. **Kostka, G., R. Giltay, W. Bloch, K. Addicks, R. Timpl, R. Fassler, and M. L. Chu.** 2001. Perinatal lethality and endothelial cell abnormalities in several vessel compartments of fibulin-1-deficient mice. Mol. Cell. Biol. **21:**7025–7034.
26. **Kozel, B. A., H. Wachi, E. C. Davis, and R. P. Mecham.** 2003. Domains in tropoelastin that mediate elastin deposition in vitro and in vivo. J. Biol. Chem. **278:**18491–18498.
27. **Li, D. Y., B. Brooke, E. C. Davis, R. P. Mecham, L. K. Sorensen, B. B. Boak, E. Eichwald, and M. T. Keating.** 1998. Elastin is an essential determinant of arterial morphogenesis. Nature **393:**276–280.
28. **Liu, X., Y. Zhao, J. Gao, B. Pawlyk, B. Starcher, J. A. Spencer, H. Yanagisawa, J. Zuo, and T. Li.** 2004. Elastic fiber homeostasis requires lysyl oxidase-like 1 protein. Nat. Genet. **36:**178–182.
29. **Loeys, B., L. Van Maldergem, G. Mortier, P. Coucke, S. Gerniers, J. M. Naeyaert, and A. De Paepe.** 2002. Homozygosity for a missense mutation in fibulin-5 (FBLN5) results in a severe form of cutis laxa. Hum. Mol. Genet. **11:**2113–2118.
30. **Maki, J. M., and K. I. Kivirikko.** 2001. Cloning and characterization of a fourth human lysyl oxidase isoenzyme. Biochem. J. **355:**381–387.
31. **Maki, J. M., J. Rasanen, H. Tikkanen, R. Sormunen, K. Makikallio, K. I. Kivirikko, and R. Soininen.** 2002. Inactivation of the lysyl oxidase gene Lox leads to aortic aneurysms, cardiovascular dysfunction, and perinatal death in mice. Circulation **106:**2503–2509.
32. **Markova, D., Y. Zou, F. Ringpfeil, T. Sasaki, G. Kostka, R. Timpl, J. Uitto, and M. L. Chu.** 2003. Genetic heterogeneity of cutis laxa: a heterozygous tandem duplication within the fibulin-5 (FBLN5) gene. Am. J. Hum. Genet. **72:**998–1004.
33. **Marmorstein, A. D., L. Y. Marmorstein, M. Rayborn, X. Wang, J. G. Hollyfield, and K. Petrukhin.** 2000. Bestrophin, the product of the Best vitelliform macular dystrophy gene (*VMD2*), localizes to the basolateral plasma membrane of the retinal pigment epithelium. Proc. Natl. Acad. Sci. USA **97:**12758–12763.

34. **Marmorstein, L. Y., A. V. Kinev, G. K. Chan, D. A. Bochar, H. Beniya, J. A. Epstein, T. J. Yen, and R. Shiekhattar.** 2001. A human BRCA2 complex containing a structural DNA binding component influences cell cycle progression. Cell **104**:247–257.
35. **Marmorstein, L. Y., P. J. McLaughlin, J. B. Stanton, L. Yan, J. W. Crabb, and A. D. Marmorstein.** 2002. Bestrophin interacts physically and functionally with protein phosphatase 2A. J. Biol. Chem. **277**:30591–30597.
36. **Marmorstein, L. Y., F. L. Munier, Y. Arsenijevic, D. F. Schorderet, P. J. McLaughlin, D. Chung, E. Traboulsi, and A. D. Marmorstein.** 2002. Aberrant accumulation of EFEMP1 underlies drusen formation in malattia leventinese and age-related macular degeneration. Proc. Natl. Acad. Sci. USA **99**:13067–13072.
37. **Mecham, R. P., and E. Davis.** 1994. Elastic fiber structure and assembly, p. 281–314. *In* P. D. Yurchenco, D. E. Birk, and R. P. Mecham (ed.), Extracellular matrix assembly and structure. Academic Press, New York, N.Y.
38. **Midwood, K. S., and J. E. Schwarzbauer.** 2002. Elastic fibers: building bridges between cells and their matrix. Curr. Biol. **12**:R279–R281.
39. **Milewicz, D. M., Z. Urban, and C. Boyd.** 2000. Genetic disorders of the elastic fiber system. Matrix Biol. **19**:471–480.
40. **Nakamura, T., P. R. Lozano, Y. Ikeda, Y. Iwanaga, A. Hinek, S. Minamisawa, C. F. Cheng, K. Kobuke, N. Dalton, Y. Takada, K. Tashiro, J. Ross, Jr., T. Honjo, and K. R. Chien.** 2002. Fibulin-5/DANCE is essential for elastogenesis in vivo. Nature **415**:171–175.
41. **Pasquali-Ronchetti, I., and M. Baccarani-Contri.** 1997. Elastic fiber during development and aging. Microsc. Res. Tech. **38**:428–435.
42. **Pereira, L., K. Andrikopoulos, J. Tian, S. Y. Lee, D. R. Keene, R. Ono, D. P. Reinhardt, L. Y. Sakai, N. J. Biery, T. Bunton, H. C. Dietz, and F. Ramirez.** 1997. Targetting of the gene encoding fibrillin-1 recapitulates the vascular aspect of Marfan syndrome. Nat. Genet. **17**:218–222.
43. **Pereira, L., S. Y. Lee, B. Gayraud, K. Andrikopoulos, S. D. Shapiro, T. Bunton, N. J. Biery, H. C. Dietz, L. Y. Sakai, and F. Ramirez.** 1999. Pathogenetic sequence for aneurysm revealed in mice underexpressing fibrillin-1. Proc. Natl. Acad. Sci. USA **96**:3819–3823.
44. **Pierce, R. A., T. J. Mariani, and R. M. Senior.** 1995. Elastin in lung development and disease. Ciba Found. Symp. **192**:199–212.
45. **Reinboth, B., E. Hanssen, E. G. Cleary, and M. A. Gibson.** 2002. Molecular interactions of biglycan and decorin with elastic fiber components: biglycan forms a ternary complex with tropoelastin and microfibril-associated glycoprotein 1. J. Biol. Chem. **277**:3950–3957.
46. **Rosenbloom, J., W. R. Abrams, and R. Mecham.** 1993. Extracellular matrix 4: the elastic fiber. FASEB J. **7**:1208–1218.
47. **Schultz, D. W., M. L. Klein, A. J. Humpert, C. W. Luzier, V. Persun, M. Schain, A. Mahan, C. Runckel, M. Cassera, V. Vittal, T. M. Doyle, T. M. Martin, R. G. Weleber, P. J. Francis, and T. S. Acott.** 2003. Analysis of the ARMD1 locus: evidence that a mutation in HEMICENTIN-1 is associated with age-related macular degeneration in a large family. Hum. Mol. Genet **12**:3315–3323.
48. **Scott, J. E.** 1980. Collagen-proteoglycan interactions. Localization of proteoglycans in tendon by electron microscopy. Biochem. J. **187**:887–891.
49. **Starcher, B., and M. Conrad.** 1995. A role for neutrophil elastase in the progression of solar elastosis. Connect. Tissue Res. **31**:133–140.
50. **Stone, E. M., T. A. Braun, S. R. Russell, M. H. Kuehn, A. J. Lotery, P. A. Moore, C. G. Eastman, T. L. Casavant, and V. C. Sheffield.** 2004. Missense variations in the fibulin 5 gene and age-related macular degeneration. N. Engl. J. Med. **351**:346–353.
51. **Stone, E. M., A. J. Lotery, F. L. Munier, E. Heon, B. Piguet, R. H. Guymer, K. Vandenburgh, P. Cousin, D. Nishimura, R. E. Swiderski, G. Silvestri, D. A. Mackey, G. S. Hageman, A. C. Bird, V. C. Sheffield, and D. F. Schorderet.** 1999. A single EFEMP1 mutation associated with both malattia leventinese and Doyne honeycomb retinal dystrophy. Nat. Genet. **22**:199–202.
52. **Timpl, R., T. Sasaki, G. Kostka, and M. L. Chu.** 2003. Fibulins: a versatile family of extracellular matrix proteins. Nat Rev. Mol. Cell Biol. **4**:479–489.
53. **Trask, B. C., T. M. Trask, T. Broekelmann, and R. P. Mecham.** 2000. The microfibrillar proteins MAGP-1 and fibrillin-1 form a ternary complex with the chondroitin sulfate proteoglycan decorin. Mol. Biol. Cell **11**:1499–1507.
54. **Trask, T. M., B. C. Trask, T. M. Ritty, W. R. Abrams, J. Rosenbloom, and R. P. Mecham.** 2000. Interaction of tropoelastin with the amino-terminal domains of fibrillin-1 and fibrillin-2 suggests a role for the fibrillins in elastic fiber assembly. J. Biol. Chem. **275**:24400–24406.
55. **Wu, W. J., B. Vrhovski, and A. S. Weiss.** 1999. Glycosaminoglycans mediate the coacervation of human tropoelastin through dominant charge interactions involving lysine side chains. J. Biol. Chem. **274**:21719–21724.
56. **Yanagisawa, H., E. C. Davis, B. C. Starcher, T. Ouchi, M. Yanagisawa, J. A. Richardson, and E. N. Olson.** 2002. Fibulin-5 is an elastin-binding protein essential for elastic fibre development in vivo. Nature **415**:168–171.

Matrix Metalloproteinase-9 Promoter Polymorphism Associated with Upper Lung Dominant Emphysema

Isao Ito, Sonoko Nagai, Tomohiro Handa, Shigeo Muro, Toyohiro Hirai, Mitsuhiro Tsukino, and Michiaki Mishima

Department of Respiratory Medicine, Graduate School of Medicine, Kyoto University, Kyoto, Japan

Rationale: **Matrix metalloproteinase 9 (MMP-9) has proteolytic activity against connective tissue proteins and appears to play an important role in the development of chronic obstructive pulmonary disease (COPD). The functional polymorphism of MMP-9 (C-1562T) is considered as one of the candidate genes in the susceptibility to COPD.**

Objectives: **To determine if MMP-9 (C-1562T) is related to the development of COPD in the Japanese population and whether it is associated with development of pulmonary emphysema assessed by high-resolution computed tomographic (HRCT) parameters.**

Methods: **MMP-9 (C-1562T) genotypes of 84 patients with COPD and 85 healthy smokers (control subjects) were determined by the restriction fragment length polymorphism method. We investigated the relationship between the genotypes using automatically analyzed HRCT parameters, such as percentage of low attenuation area (LAA%) and average computed tomography (CT) value density (Hounsfield units; mean CTv) in upper, middle, and lower lung fields in all patients with COPD.**

Measurements and Main Results: **There was no difference in polymorphism of MMP-9 (C-1562T) between patients with COPD and control subjects. In the HRCT study, patients with COPD with a T allele (C/T or T/T) showed larger LAA% (95% confidence interval of difference, 0.5–18.7; $p = 0.04$), and smaller mean CTv (confidence interval, −34.3 to −1.0; $p = 0.04$) in the upper lung compared with patients without T alleles (C/C). However, pulmonary function tests showed no difference between the two patient groups. Patients with a T allele showed a decrease in LAA% and an increase in mean CTv from upper to lower lung fields ($p = 0.006$ and $p = 0.002$, respectively).**

Conclusions: **Polymorphism of MMP-9 (C-1562T) was associated with upper lung dominant emphysema in patients with COPD.**

Keywords: chronic obstructive pulmonary disease; high-resolution computed tomography; low attenuation area %; mean CT value

Chronic obstructive pulmonary disease (COPD) is characterized by decreased expiratory flow rates. The most significant factor for developing COPD is cigarette smoking (1). However, it is estimated that only 15 to 20% of chronic smokers develop this disease, which is characterized by rapid decline of FEV_1 (2, 3). There are several epidemiologic studies that demonstrate familial clustering of the disease (4, 5). These facts suggest that genetic factors have a role in contributing to an individual's susceptibility to COPD. Of the candidate genes investigated in relation to COPD development, those coding for matrix metalloproteinases (MMPs) have attracted attention under the widely accepted protease–antiprotease imbalance theory associated with the pathogensis of this disease (6–12).

MMP-9, also called gelatinase B, has been proposed to play a role in the development of emphysema and is involved in the digestion of extracellular matrix components such as gelatin, collagens (IV, V, XI, XVII), and elastin (13). The human MMP-9 gene is located on chromosome 20q11.1–13.1, and MMP-9 is synthesized as a proenzyme with a molecular mass of 92 kD. Among several polymorphic changes reported in the regulatory region (14, 15), the C-1562T polymorphism increases the promoter activity of MMP-9 (16, 17). This polymorphism was shown to have a possible role in development of atherosclerotic diseases (16, 18, 19). In COPD, there are few studies investigating the relationship of the polymorphism to the development of the disease (20–22). Minematsu and colleagues evaluated the degree of emphysematous changes by a visual scoring system using conventional computed tomography (CT) in a Japanese population, and found that smokers with the T allele showed more severe emphysema than smokers without the T allele (20). Zhou and colleagues showed that C-1562T was more frequent in patients with COPD diagnosed by pulmonary function tests, compared with control subjects in a Chinese population (22). However, Joos and colleagues reported that fast decline of FEV_1 was not related to the polymorphism among white smokers (21). Thus, the role of the MMP-9 C-1562T polymorphism in association with COPD has been assessed by a variety of methods and the issue remains inconclusive.

To test the hypothesis that the MMP-9 C-1562T polymorphism has an important role in susceptibility to developing COPD, we first analyzed the polymorphisms in a sample of patients with COPD and healthy smokers (control subjects) from the Japanese population. Automatically calculated parameters, such as percentage of low attenuation area (LAA%) and mean CT value (mean CTv) in high-resolution CT (HRCT), have previously been shown to be useful in assessment of the emphysema-associated parenchymal injuries seen in patients with COPD (23–26). Second, using radiologic parameters assessed by HRCT, we examined patients with COPD for the correlation between the genotypes and phenotypes of emphysema.

METHODS

Subjects

The study comprised 84 patients with COPD and 85 healthy smokers. The subjects were included according to criteria established in previous studies (26, 27), with minor modifications. Briefly, COPD was diagnosed according to the Global Initiative for Obstructive Lung Disease (GOLD) guidelines (28), and no patient with α_1-antitrypsin deficiency was included. This study was approved by the ethics committee of Kyoto University, and written, informed consent was obtained from all subjects.

Genotyping

A standard phenol-chloroform method was used to extract DNA from blood. Polymerase chain reaction (PCR) followed by restriction fragment length polymorphism analysis were performed to detect a point

(Received in original form June 20, 2005; accepted in final form August 26, 2005)

Correspondence and requests for reprints should be addressed to Sonoko Nagai, M.D., Ph.D., Department of Respiratory Medicine, Graduate School of Medicine, Kyoto University, Shogoin-kawaharacho 54, Sakyo-ku, Kyoto, 606-8507, Japan. E-mail: nagai@kuhp.kyoto-u.ac.jp

Am J Respir Crit Care Med Vol 172. pp 1378–1382, 2005
Originally Published in Press as DOI: 10.1164/rccm.200506-953OC on August 26, 2005
Internet address: www.atsjournals.org

TABLE 1. BASELINE CHARACTERISTICS OF STUDY SUBJECTS

	Men/Women	Age (*yr*)	Smoking History (*pack-yr*)	FVC (*L*)	FEV_1 (*%pred*)	FEV_1/FVC (%)
Patients with COPD, n = 84	81/3	68.9 ± 7.5	58.1 ± 28.9	2.58 ± 0.80	44.9 ± 17.4	45.3 ± 9.8
Control smokers, n = 85	69/16	58.8 ± 12.8	41.4 ± 22.4	3.33 ± 1.11	88.5 ± 20.9	80.2 ± 7.9

Definition of abbreviation: COPD = chronic obstructive pulmonary disease.
Values are mean ± SD.

mutation at the promoter of C-1562T of the MMP-9 gene as described by Zhang and colleagues (16). PCR was performed with a thermal cycler (DNA Thermal Cycler; Perkin Elmer Cetus, Norwalk, CT) with the following cycling parameters: 94°C for 30 s, 65°C for 30 s, and 72°C for 30 s, for 35 cycles. The PCR products were digested with restriction enzyme *Bbu* I (Takara Bio, Otsu, Japan) at 37°C for 4 h, resolved on 3% agarose gels, stained with ethidium bromide (Invitrogen, Carlsbad, CA), and observed under ultraviolet light.

Measurement of Chest HRCT Parameters in Patients with COPD

All CT images were taken on subjects in the supine position with an HRCT scanner (X-Vigor; Toshiba, Tokyo, Japan), with 2-mm collimation according to the previously reported protocol (23–26). Three images were used for analysis for each patient: upper lung field at 1 cm above the upper margin of the aortic arch, middle lung at 1 cm below the carina, and lower lung at 3 cm above the diaphragm (23, 25). Contiguous pixels with less than −960 Hounsfield units (HU) were defined as LAA and the percentage ratio of LAA in both lung fields on each images (LAA%) was calculated automatically (23, 25): LAA-U%, at the upper lung field; LAA-M%, at the middle; LAA-L%, at the lower; and LAA-T%, for the average of the three images. LAA-T% was calculated as Σ(LAA-X% × no. of lung pixels in X)/(total no. of pixels of lung fields in three images). Mean CTv-U, mean CTv-M, and mean CTv-L were calculated as the average of the CT values in HU of all pixels in both lung fields at the upper, middle, and lower lung fields, respectively. Mean CTv-T was defined described for LAA-T%.

Statistical Analysis

To test frequencies of the MMP-9 C-1562T polymorphism, χ^2 tests for the equality of two population probabilities were performed. A two-tailed *t* test was used to test the difference of averages in the pulmonary function tests and the HRCT parameters between T(+) subjects (with C/C genotype) and T(−) subjects (with C/T or T/T genotype). Analysis of variance (ANOVA) with repeated measures was used to explore the effect of image levels on HRCT parameters separately for each patient group. For multiple comparisons, a *post hoc* test with Bonferroni/Dunn's method was used. StatView version 5.0 (SAS Institute, Inc., Cary, NC) was used for the calculations. p values less than 0.05 were considered to be significant.

RESULTS

The baseline characteristics and the results of the pulmonary function tests for the 84 patients with COPD and 85 control subjects (healthy smokers) are presented in Table 1. In the initial evaluation of patients with COPD, two patients were classified as having stage I disease, 33 as having stage II, 30 as having stage III, and 19 as having stage IV disease, according to the revised GOLD criteria (28).

The genotype frequencies in each group are shown in Table 2. There were no significant differences in frequencies of alleles and genotypes between patients with COPD and control subjects. Because the T allele has a codominant effect on plasma MMP-9 level (17), we divided patients with COPD and control subjects into two groups for comparison of clinical parameters between genotypes: T(−) subjects (with C/C genotype) and T(+) subjects (with C/T or T/T genotype). Pulmonary functions were not significantly different between the T(+)and T(−)groups among either patients with COPD (Table 3) or control subjects (data not shown).

Chest HRCT examination was performed to obtain HRCT parameters in all patients with COPD. Results of LAA% and mean CTv calculated in each genotype group are shown in Figures 1 and 2. Although LAA-M%, LAA-L%, and LAA-T% between T(−) and T(+) patients were not significantly different (p = 0.23, 0.45, and 0.15, respectively), LAA-U% was notably higher in T(+) patients than in T(−) patients (95% confidence interval [CI], 0.5–18.7; p = 0.04; Figure 1). In the measurement of mean CTv, mean CTv-U was considerably lower in T(+) patients than in T(−) patients (95% CI, −34.3 to −1.0; p = 0.04), whereas mean CTv-M, mean CTv-L, and mean CTv-T were not significantly different (p = 0.28, 0.70, and 0.20, respectively; Figure 2). In comparisons among the three image positions in each patient group by ANOVA with repeated measures, LAA% in T(+) patients significantly decreased as the positions of the images moved from upper to lower (p = 0.006), whereas LAA% in T(−) patients did not change (p = 0.53; Figure 1). Mean CTv in T(+) patients significantly increased as the positions moved from upper to lower (p = 0.002), whereas mean CTv in T(−) patients did not change (p = 0.32; Figure 2). There was no significant difference between patients with T/T genotype and patients with C/T genotype in any HRCT parameters (data not shown).

DISCUSSION

This study demonstrated that the T allele at the MMP-9 C-1562T polymorphism was significantly associated with upper lung dominant emphysema in patients with COPD, although the polymorphism was not associated with the development of COPD in the Japanese population. Previous studies reporting on the association of this polymorphism with the risk of developing COPD have shown variable results (20–22). Our results corroborate those of Minematsu and colleagues (20), showing that the T allele has some role in the progression of emphysema in lung parenchyma, at least in the Japanese population. We reported that T(+) patients are linked with upper lung dominant emphysema but not with further deterioration of lung function, compared with T(−) patients. In addition, our data show this polymorphism to have

TABLE 2. ALLELIC AND GENOTYPIC FREQUENCIES IN PATIENTS WITH CHRONIC OBSTRUCTIVE PULMONARY DISEASE AND HEALTHY CONTROL SMOKERS

	COPD (*n = 84*)	Control (*n = 85*)	p Value
Allele			
C	145 (86%)	144 (85%)	0.79
T	23 (14%)	26 (15%)	
Genotype			
CC	63 (75%)	60 (71%)	0.61
CT	19 (23%)	24 (28%)	
TT	2 (2%)	1 (1%)	

For definition of abbreviation, *see* Table 1.

TABLE 3. COMPARISON OF PULMONARY FUNCTIONS BETWEEN T(−) PATIENTS AND T(+) PATIENTS, BOTH WITH CHRONIC OBSTRUCTIVE PULMONARY DISEASE

	Men/Women	Age (*yr*)	Smoking History (*pack-yr*)	FVC (*L*)	FEV_1 (*%pred*)	FEV_1/FVC (%)	D_{LCO}/V_A*
T(−) patients, n = 63	60/3	68.2 ± 7.6	59.2 ± 29.6	2.55 ± 0.82	44.4 ± 17.4	45.3 ± 9.7	3.50 ± 1.41
T(+) patients, n = 21	21/0	70.7 ± 6.7	54.7 ± 29.5	2.67 ± 0.70	46.3 ± 16.9	45.1 ± 10.0	2.96 ± 1.11
p Value		0.19	0.56	0.54	0.67	0.92	0.14

Definition of abbreviation: D_{LCO}/V_A = diffusing capacity of the lung for carbon monoxide per unit of alveolar volume.
Values are mean ± SD.
* Nos. of patients measured are 51 in T(−) group and 19 in T(+) group.

no association with an increased risk of COPD development, determined by the decreased value of FEV_1/FVC and not by radiographic evaluation, and has some accordance with the result by Joos and colleagues, who evaluated the risk by fast rate of FEV_1 decline (21). We believe that discrepancies in the role of the T allele between the HRCT findings and pulmonary function are due to emphysematous change in the upper lung having less influence on the decrease of FEV_1 than the influence of emphysema in the lower lung (29).

Two major types of parenchymal destruction in pulmonary emphysema are differentiated in the general population, and are described as centrilobular emphysema and panlobular emphysema (26, 30–32). Centrilobular emphysema begins in and around the respiratory bronchioles, resulting in dilatation and destruction of the lobule center. A predilection of centrilobular emphysema for the upper lung, rather than lower lung, has been noted. Panlobular emphysema, also referred to as panacinar emphysema, affects the acinus of the entire secondary lobule. This latter type of emphysema extends diffusely throughout the lung, with some preferential involvement in the lower lung. In addition to the histopathologic differences, differences in pathophysiology, such as elasticity (33) and airway reactivity (34), between the two types of emphysema have been noted in smokers. Because the phenotypes for centrilobular and panlobular emphysema are different, there could also be differences between the progressions of the two types of emphysema. Because we did not investigate lung pathology of patients with COPD, we were not able to differentiate the two types of emphysema in our subjects. Considering that centrilobular emphysema is the dominant type linked to cigarette smoking, it does not seem adequate to interpret the presence or absence of the T allele as simply corresponding to the centrilobular or panlobular type of emphysema.

Few attempts have been made to investigate a link between genetic factors and emphysematous changes in HRCT (26, 35). A correlation study between HRCT and the pathologic findings used to discriminate between the two types of emphysema is needed to develop a protocol for using HRCT to discriminate between the two types. It would then be possible to determine the mechanism whereby the MMP-9 promoter C-1562T polymorphism contributes to the development of upper lung dominant emphysema. Most patients with COPD in our study had stage II–IV disease, and only a very few had stage 0–I. It would extend our results to use HRCT to investigate patients with 0–I stage disease to determine whether this polymorphism contributes to early development of upper lung dominant emphysema; this is difficult to detect by pulmonary function tests.

The primary mechanism of lung parenchymal destruction is believed to be an imbalance between endogenous proteinases and antiproteinases. The significant biological function of MMP-9, which is related to destruction of lung parenchyma, is considered to be due to its proteolytic effect on substrates such as extracellular matrix proteins and antiproteinases. Although the two types of emphysema may show similar distributions within the lung during advanced disease stages, and may sometimes coexist (30, 36), there is believed to be some difference in the way proteinase–antiproteinase imbalance affects the progression of emphysema (37).

MMP-9 is expressed by many kinds of inflammatory cells, such as alveolar macrophages, neutrophils, and eosinophils (13). Among them, alveolar macrophages are likely to have an important pathogenic role in emphysema (38, 39). This protein is also produced by structural cells in the lung, such as bronchial epithelial cells, alveolar type II cells, and smooth muscle cells, in appropriate conditions (13). The role of MMP-9 has been

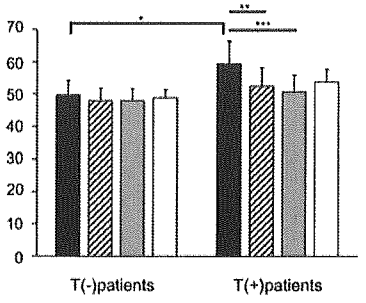

Figure 1. Percentage of low attenuation area (LAA%) in T(+) and T(−) patients. *Black bars* denote LAA% in the upper lung (LAA-U%), *hatched bars* denote LAA% in the middle lung (LAA-M%), *gray bars* denote LAA% in the lower lung (LAA-L%), and *white bars* denote LAA% for the average of the three lung fields (LAA-T%). *Error bars* depict the 95% confidence interval. **Bracket* shows comparison and significant difference in LAA-U% between T(+) and T(−) patients ($p = 0.04$). By analysis of variance (ANOVA) with repeated measures, there was a significant effect of slice position of high-resolution computed tomography (HRCT) among T(+) patients ($p = 0.006$), but not in T(−) patients ($p = 0.53$). **$p = 0.01$; ***$p < 0.01$.

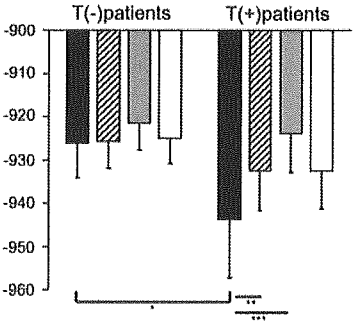

Figure 2. Mean computed tomographic (CT) value (mean CTv) in T(+) and T(−) patients. *Black bars* denote mean CTv in the upper lung (mean CTv-U), *hatched bars* denote mean CTv in the middle lung (mean CTv-M), *gray bars* denote mean CTv in the lower lung (mean CTv-L), and *white bars* denote mean CTv for the average of the three lung fields (mean CTv-T). *Error bars* depict the 95% confident interval. **Bracket* shows comparison and significant difference in mean CTv-U between T(+) and T(−) patients ($p = 0.04$). By ANOVA with repeated measures, there was a significant effect of slice position of HRCT among T(+) patients ($p = 0.002$), but not in T(−) patients ($p = 0.32$). **$p < 0.05$; ***$p < 0.001$.

shown to be important in the development of emphysema in animal (40–44) and human (6, 7, 9–12, 39, 45, 46) studies. Histopathologically, MMP-1, MMP-2, MMP-8, and MMP-9 showed increased expression in the lungs of patients with COPD (9). However, mRNA of MMP-1, not MMP-9 or MMP-12, was expressed more in the lungs of patients with severe emphysema than in those of normal subjects (47). In murine models of emphysema induced by chronic cigarette smoke, Churg and colleagues emphasized the relevance of MMP-12 in relation to tumor necrosis factor α (48). Thus, there is debate that other MMPs may also play important roles in the destruction of alveolar walls.

Why some patients with COPD present upper lung dominant emphysema and how the T allele of the MMP-9 promoter is related to this phenotype is still unknown and requires further study. Considering that C-1562T polymorphism increases the promoter activity (16, 17), it could be inferred that MMP-9 activity plays a more important role in the destruction of alveolar walls in the upper lung than in the lower lung. Because MMP-9 alone does not digest collagen type I/III, which is the primary element of alveolar walls sustaining the mechanical force of breathing (49, 50), other enzymes mentioned above may also be preferentially expressed in the upper lung, and collaborate with MMP-9 in the digestion of the extracellular matrix. After proteolytic digestion of the extracellular matrix, with resultant weakened remodeling of the collagen network, mechanical force plays an important role in destroying alveolar walls (49–51). Distribution of the mechanical stress is larger in the upper lung due to the overall weight of the lung (52), and could contribute to the preferential progression of emphysema in the upper lung of certain patients. Our data suggest that, in a Japanese population with COPD, the C-1562T polymorphism could affect the distribution and the progression of emphysema, not the susceptibility to COPD (decline of FEV_1).

In conclusion, we have shown that C-1562T polymorphism in the MMP-9 promoter was not associated with development of COPD diagnosed by pulmonary function tests. However, the T allele was significantly associated with the development of upper lung dominant emphysema in patients with COPD. The role of MMP-9 promoter genotypes in the progression of emphysema remains to be elucidated.

Conflict of Interest Statement: None of the authors have a financial relationship with a commercial entity that has an interest in the subject of this manuscript.

Acknowledgment: The authors thank Professor Kimio Morimune, the Graduate School of Economics, Kyoto University, for his help in statistical analyses, and Dr. Koichi Nishimura, Department of Respiratory Medicine, Kyoto University Hospital, for his clinical work on patients with COPD and for providing the clinical data. They also thank Zöe Müller, B.Sc., and Sarah Foley for their English editing.

References

1. Snider GL. Chronic obstructive pulmonary disease: risk factors, pathophysiology and pathogenesis. *Annu Rev Med* 1989;40:411–429.
2. Hoshino Y, Nagai S, Koyama H, Okuda K, Nishimura K, Miki H, Hamada K, Izumi T. Airflow limitation in Japanese smokers: significance of serum neutrophil elastase/α1 -proteinase inhibitor ratio and FEV1 (% pred.) adjusted by pack-years. *Respiration (Herrlisheim)* 2000; 67:372–377.
3. Fletcher C, Peto R. The natural history of chronic airflow obstruction. *BMJ* 1977;1:1645–1648.
4. Khoury MJ, Beaty TH, Newill CA, Bryant S, Cohen BH. Genetic-environmental interactions in chronic airways obstruction. *Int J Epidemiol* 1986;15:65–72.
5. Kueppers F, Miller RD, Gordon H, Hepper NG, Offord K. Familial prevalence of chronic obstructive pulmonary disease in a matched pair study. *Am J Med* 1977;63:336–342.
6. Ohnishi K, Takagi M, Kurokawa Y, Satomi S, Konttinen YT. Matrix metalloproteinase-mediated extracellular matrix protein degradation in human pulmonary emphysema. *Lab Invest* 1998;78:1077–1087.
7. Betsuyaku T, Nishimura M, Takeyabu K, Tanino M, Venge P, Xu S, Kawakami Y. Neutrophil granule proteins in bronchoalveolar lavage fluid from subjects with subclinical emphysema. *Am J Respir Crit Care Med* 1999;159:1985–1991.
8. Lim S, Roche N, Oliver BG, Mattos W, Barnes PJ, Chung KF. Balance of matrix metalloprotease-9 and tissue inhibitor of metalloprotease-1 from alveolar macrophages in cigarette smokers: regulation by interleukin-10. *Am J Respir Crit Care Med* 2000;162:1355–1360.
9. Segura-Valdez L, Pardo A, Gaxiola M, Uhal BD, Becerril C, Selman M. Upregulation of gelatinases A and B, collagenases 1 and 2, and increased parenchymal cell death in COPD. *Chest* 2000;117:684–694.
10. Russell RE, Culpitt SV, DeMatos C, Donnelly L, Smith M, Wiggins J, Barnes PJ. Release and activity of matrix metalloproteinase-9 and tissue inhibitor of metalloproteinase-1 by alveolar macrophages from patients with chronic obstructive pulmonary disease. *Am J Respir Cell Mol Biol* 2002;26:602–609.
11. Mao JT, Tashkin DP, Belloni PN, Baileyhealy I, Baratelli F, Roth MD. All-trans retinoic acid modulates the balance of matrix metalloproteinase-9 and tissue inhibitor of metalloproteinase-1 in patients with emphysema. *Chest* 2003;124:1724–1732.
12. Beeh KM, Beier J, Kornmann O, Buhl R. Sputum matrix metalloproteinase-9, tissue inhibitor of metalloprotinease-1, and their molar ratio in patients with chronic obstructive pulmonary disease, idiopathic pulmonary fibrosis and healthy subjects. *Respir Med* 2003;97:634–639.
13. Atkinson JJ, Senior RM. Matrix metalloproteinase-9 in lung remodeling. *Am J Respir Cell Mol Biol* 2003;28:12–24.
14. Zhang B, Henney A, Eriksson P, Hamsten A, Watkins H, Ye S. Genetic variation at the matrix metalloproteinase-9 locus on chromosome 20q12.2–13.1. *Hum Genet* 1999;105:418–423.
15. Hirakawa S, Lange EM, Colicigno CJ, Freedman BI, Rich SS, Bowden DW. Evaluation of genetic variation and association in the matrix metalloproteinase 9 (MMP9) gene in ESRD patients. *Am J Kidney Dis* 2003;42:133–142.
16. Zhang B, Ye S, Herrmann SM, Eriksson P, de Maat M, Evans A, Arveiler D, Luc G, Cambien F, Hamsten A, *et al.* Functional polymorphism in the regulatory region of gelatinase B gene in relation to severity of coronary atherosclerosis. *Circulation* 1999;99:1788–1794.
17. Blankenberg S, Rupprecht HJ, Poirier O, Bickel C, Smieja M, Hafner G, Meyer J, Cambien F, Tiret L; AtheroGene Investigators. Plasma concentrations and genetic variation of matrix metalloproteinase 9 and prognosis of patients with cardiovascular disease. *Circulation* 2003;107:1579–1585.
18. Jones GT, Phillips VL, Harris EL, Rossaak JI, van Rij AM. Functional matrix metalloproteinase-9 polymorphism (C-1562T) associated with abdominal aortic aneurysm. *J Vasc Surg* 2003;38:1363–1367.
19. Morgan AR, Zhang B, Tapper W, Collins A, Ye S. Haplotypic analysis of the MMP-9 gene in relation to coronary artery disease. *J Mol Med* 2003;81:321–326.
20. Minematsu N, Nakamura H, Tateno H, Nakajima T, Yamaguchi K. Genetic polymorphism in matrix metalloproteinase-9 and pulmonary emphysema. *Biochem Biophys Res Commun* 2001;289:116–119.
21. Joos L, He JQ, Shepherdson MB, Connett JE, Anthonisen NR, Pare PD, Sandford AJ. The role of matrix metalloproteinase polymorphisms in the rate of decline in lung function. *Hum Mol Genet* 2002;11:569–576.
22. Zhou M, Huang SG, Wan HY, Li B, Deng WW, Li M. Genetic polymorphism in matrix metalloproteinase-9 and the susceptibility to chronic obstructive pulmonary disease in Han population of south China. *Chin Med J (Engl)* 2004;117:1481–1484.
23. Sakai N, Mishima M, Nishimura K, Itoh H, Kuno K. An automated method to assess the distribution of low attenuation areas on chest CT scans in chronic pulmonary emphysema patients. *Chest* 1994;106: 1319–1325.
24. Mishima M, Hirai T, Itoh H, Nakano Y, Sakai H, Muro S, Nishimura K, Oku Y, Chin K, Ohi M, *et al.* Complexity of terminal airspace geometry assessed by lung computed tomography in normal subjects and patients with chronic obstructive pulmonary disease. *Proc Natl Acad Sci USA* 1999;96:8829–8834.
25. Mishima M, Oku Y, Kawakami K, Sakai N, Fukui M, Hirai T, Chin K, Ohi M, Nishimura K, Itoh H, *et al.* Quantitative assessment of the spatial distribution of low attenuation areas on X-ray CT using texture analysis in patients with chronic pulmonary emphysema. *Front Med Biol Eng* 1997;8:19–34.
26. Ito I, Nagai S, Hoshino Y, Muro S, Hirai T, Tsukino M, Mishima M. Risk and severity of COPD is associated with the group-specific component of serum globulin 1F allele. *Chest* 2004;125:63–70.
27. Nakano Y, Muro S, Sakai H, Hirai T, Chin K, Tsukino M, Nishimura K, Itoh H, Pare PD, Hogg JC, *et al.* Computed tomographic measurements

of airway dimensions and emphysema in smokers: correlation with lung function. *Am J Respir Crit Care Med* 2000;162:1102–1108.
28. GOLD. Global inititiative for chronic obstructive lung disease. Workshop report: global strategy for the diagnosis, management and prevention of COPD. Bethesda, MD: National Institutes for Health; 2004; [accessed 8 Sept 2004]. Available from: http://www.goldcopd.com.
29. Saitoh T, Koba H, Shijubo N, Tanaka H, Sugaya F. Lobar distribution of emphysema in computed tomographic densitometric analysis. *Invest Radiol* 2000;35:235–243.
30. Hogg JC. Pathophysiology of airflow limitation in chronic obstructive pulmonary disease. *Lancet* 2004;364:709–721.
31. Anderson AE Jr, Foraker AG. Centrilobular emphysema and panlobular emphysema: two different diseases. *Thorax* 1973;28:547–550.
32. Thurlbeck WM. The incidence of pulmonary emphysema, with observations on the relative incidence and spatial distribution of various types of emphysema. *Am Rev Respir Dis* 1963;87:206–215.
33. Kim WD, Eidelman DH, Izquierdo JL, Ghezzo H, Saetta MP, Cosio MG. Centrilobular and panlobular emphysema in smokers: two distinct morphologic and functional entities. *Am Rev Respir Dis* 1991;144:1385–1390.
34. Finkelstein R, Ma HD, Ghezzo H, Whittaker K, Fraser RS, Cosio MG. Morphometry of small airways in smokers and its relationship to emphysema type and hyper-responsiveness. *Am J Respir Crit Care Med* 1995;152:267–276.
35. Sakao S, Tatsumi K, Igari H, Watanabe R, Shino Y, Shirasawa H, Kuriyama T. Association of tumor necrosis factor-alpha gene promoter polymorphism with low attenuation areas on high-resolution CT in patients with COPD. *Chest* 2002;122:416–420.
36. Mitchell RS, Silvers GW, Goodman N, Dart G, Maisel JC. Are centrilobular emphysema and panlobular emphysema two different diseases? *Hum Pathol* 1970;1:433–441.
37. Cockcroft DW, Horne SL. Localization of emphysema within the lung: an hypothesis based upon ventilation/perfusion relationships. *Chest* 1982;82:483–487.
38. Finkelstein R, Fraser RS, Ghezzo H, Cosio MG. Alveolar inflammation and its relation to emphysema in smokers. *Am J Respir Crit Care Med* 1995;152:1666–1672.
39. Finlay GA, O'Driscoll LR, Russell KJ, D'Arcy EM, Masterson JB, FitzGerald MX, O'Connor CM. Matrix metalloproteinase expression and production by alveolar macrophages in emphysema. *Am J Respir Crit Care Med* 1997;156:240–247.
40. Wang Z, Zheng T, Zhu Z, Homer RJ, Riese RJ, Chapman HA Jr, Shapiro SD, Elias JA. Interferon gamma induction of pulmonary emphysema in the adult murine lung. *J Exp Med* 2000;192:1587–1600.
41. Wert SE, Yoshida M, LeVine AM, Ikegami M, Jones T, Ross GF, Fisher JH, Korfhagen TR, Whitsett JA. Increased metalloproteinase activity, oxidant production, and emphysema in surfactant protein D gene-inactivated mice. *Proc Natl Acad Sci USA* 2000;97:5972–5977.
42. Selman M, Cisneros-Lira J, Gaxiola M, Ramirez R, Kudlacz EM, Mitchell PG, Pardo A. Matrix metalloproteinases inhibition attenuates tobacco smoke-induced emphysema in Guinea pigs. *Chest* 2003;123:1633–1641.
43. Choe KH, Taraseviciene-Stewart L, Scerbavicius R, Gera L, Tuder RM, Voelkel NF. Methylprednisolone causes matrix metalloproteinase-dependent emphysema in adult rats. *Am J Respir Crit Care Med* 2003;167:1516–1521.
44. Lee JH, Lee DS, Kim EK, Choe KH, Oh YM, Shim TS, Kim SE, Lee YS, Lee SD. Simvastatin inhibits cigarette smoking-induced emphysema and pulmonary hypertension in rat lungs. *Am J Respir Crit Care Med* (In press)
45. Russell RE, Thorley A, Culpitt SV, Dodd S, Donnelly LE, Demattos C, Fitzgerald M, Barnes PJ. Alveolar macrophage-mediated elastolysis: roles of matrix metalloproteinases, cysteine, and serine proteases. *Am J Physiol Lung Cell Mol Physiol* 2002;283:L867–L873.
46. Montano M, Beccerril C, Ruiz V, Ramos C, Sansores RH, Gonzalez-Avila G. Matrix metalloproteinases activity in COPD associated with wood smoke. *Chest* 2004;125:466–472.
47. Imai K, Dalal SS, Chen ES, Downey R, Schulman LL, Ginsburg M, D'Armiento J. Human collagenase (matrix metalloproteinase-1) expression in the lungs of patients with emphysema. *Am J Respir Crit Care Med* 2001;163:786–791.
48. Churg A, Wang RD, Tai H, Wang X, Xie C, Dai J, Shapiro SD, Wright JL. Macrophage metalloelastase mediates acute cigarette smoke-induced inflammation via tumor necrosis factor-alfa release. *Am J Respir Crit Care Med* 2003;167:1083–1089.
49. Suki B, Lutchen KR, Ingenito EP. On the progressive nature of emphysema: roles of proteases, inflammation, and mechanical forces. *Am J Respir Crit Care Med* 2003;168:516–521.
50. Suki B, Ito S, Stamenovic D, Lutchen KR, Ingenito EP. Biomechanics of the lung parenchyma: critical roles of collagen and mechanical forces. *J Appl Physiol* 2005;98:1892–1899.
51. Kononov S, Brewer K, Sakai H, Cavalcante FS, Sabayanagam CR, Ingenito EP, Suki B. Roles of mechanical forces and collagen failure in the development of elastase-induced emphysema. *Am J Respir Crit Care Med* 2001;164:1920–1926.
52. West JB. Distribution of mechanical stress in the lung, a possible factor in localization of pulmonary disease. *Lancet* 1971;1:839–841.